Chemical, microphysical, and radiative effects of Indian Ocean aerosols

S. K. Satheesh,[1] V. Ramanathan,[2] B. N. Holben,[3] K. Krishna Moorthy,[4] N. G. Loeb,[5] H. Maring,[6] J. M. Prospero,[6] and D. Savoie[6]

[1] Extensive and long-term multistation measurements of aerosol properties and radiative fluxes were carried out in the haze plume off the South Asian continent. These experiments are carried out at Kaashidhoo Climate Observatory (KCO) (4.95°N, 73.5°E), Minicoy (8.5°N, 73.0°E), and Trivandrum (8.5°N, 77.0°E). In addition, the top of the atmosphere fluxes were measured simultaneously by the CERES radiation budget instrument. Long-term observations (more than 15 years) over Trivandrum show that there is a gradual increase in aerosol visible optical depth from ∼0.2 in 1986 to ∼0.4 in 1999. Pre- and post-monsoon aerosol characteristics are examined to study the seasonal variations. The impact of aerosols on short-wave radiation budget is estimated using direct observations of solar radiation using several independent ground-based radiometers and satellite data as well as from modeled aerosol properties. It was observed that "excess absorption" is not needed to model diffuse fluxes. The lower atmospheric heating due to absorbing aerosols was as high as ∼20 W m^{-2} which translates to a heating rate perturbation of ∼0.5°K/day. The effect of aerosol mixing state (internally and externally) on aerosol forcing appears to be negligible. A sensitivity study of the effect of aerosols over land in contrast to that over the ocean shows an enhancement in lower atmosphere heating by about 40% simultaneous with a reduction of ∼33% in surface cooling. Increasing sea-surface winds increase aerosol cooling due to increased sea salt aerosol concentrations, which can partly offset the heating effect due to absorbing aerosols. *INDEX TERMS:* 0305 Atmospheric Composition and Structure: Aerosols and particles (0345, 4801); 1610 Global Change: Atmosphere (0315, 0325); 1704 History of Geophysics: Atmospheric sciences; 4801 Oceanography: Biological and Chemical: Aerosols (0305); *KEYWORDS:* aerosols, radiative forcing, climate, chemical composition

1. Introduction

[2] The International Indian Ocean Experiment (INDOEX) was a field experiment in the Indian Ocean whose purpose was to assess the importance of anthropogenic aerosols from the Asian landmass on global radiative forcing and resulting solar absorption both at the Earth's surface and at the top of the atmosphere [*Ramanathan et al.*, 1995, 1996,

2001]. During INDOEX extensive observations of aerosol haze over the tropical northern Indian Ocean were carried out. The integration of INDOEX data sets, platforms and overview of the experiment are discussed by *Ramanathan et al.* [2001]. In a recent paper, *Lelieveld et al.* [2001] reported aerosols cause air quality degradation in the Asian region during winter and that the presence of aerosols may have an impact on ozone production in this region. In another paper, *Chameides et al.* [1999] examined the impact of haze (caused by aerosols) on rice and wheat production in China. They showed a decrease in solar radiation at the surface (due to aerosols) has a direct impact on rice and wheat production. They report a 5 to 30% reduction in solar radiation caused a decrease in the yield in crops in China by 5 to 30%. In addition, radiative forcing by anthropogenic aerosol particles is one of the largest sources of uncertainty in projecting climate change [*Charlson et al.*, 1992; *Kiehl and Breigleb*, 1993; *Intergovernmental Panel on Climate Change*, 1995].

[3] The INDOEX precampaign started in 1996 and results of these and the preliminary investigations made

[1]Centre for Atmospheric and Oceanic Sciences, Indian Institute of Science, Bangalore, India.
[2]Center for Clouds, Chemistry and Climate (C⁴), Scripps Institution of Oceanography, University of California, San Diego, La Jolla, California, USA.
[3]NASA Goddard Space Flight Center, Greenbelt, Maryland, USA.
[4]Space Physics Laboratory, Vikram Sarabhai Space Centre, Trivandrum, India.
[5]NASA Langley Research Center, Hampton, Virginia, USA.
[6]Rosenstiel School of Marine and Atmospheric Science, University of Miami, Miami, Florida, USA.

Table 1. Instruments Used at KCO

	Parameter Measured	Instruments Used
1	aerosol optical depth	(i) CIMEL radiometer of the AERONET[a] (340, 380, 440, 500, 670, 870, 1020 nm) (ii) Microtops radiometer (380, 440, 500, 675, 875 nm)
2	direct solar flux (W m^{-2}) (0.2–4.0 μm)	Kipp and Zonen normal incidence pyrheliometer
3	global and diffuse flux (W m^{-2}) (0.2–4.0 μm)	Kipp and Zonen pyranometer (shaded and unshaded)
4	spectral flux (W m^{-2} nm^{-1}) (0.4–1.0 μm)	spectroradiometer, analytical spectral devices
5	visible flux (W m^{-2}) (0.4–7.0 μm)	Biospherical Instruments Inc., USA.
6	aerosol scattering coefficient (534 nm)	integrating nephelometer, radiance research
7	aerosol absorption coefficient (565 nm)	particle soot/absorption photometer, radiance research
8	three-stage high volume impactor	University of Miami, Florida
9	aerosol vertical structure	(i) C-130 aircraft[b] (ii) lidar
10	TOA flux	CERES[c] radiation budget data
11	relative humidity profiles	Vaisala radio sonde
12	surface winds	R.M. Young and Co., USA

[a]AERONET stands for AErosol RObotic NETwork of NASA/GSFC.
[b]Details available at http://www.ncar.ucar.edu.
[c]CERES stands for Clouds and Earth's Radiant Energy System onboard TRMM satellite.

onboard the scientific cruises in 1996 and 1997 are available [*Moorthy et al.*, 1997; *Satheesh et al.*, 1998; *Jayaraman et al.*, 1998; *Meywerk and Ramanathan*, 1999]. The first field phase (FFP) of INDOEX took place during February and March 1998 and the intensive field phase (IFP) took place from January to March, 1999. The role of anthropogenic aerosols from Asia in modifying aerosol properties over the northern Indian Ocean and its radiative and microphysical consequences are better understood with the aid of the extensive observations carried out during the INDOEX in its both field phases. Several findings have already been reported [*Satheesh et al.*, 1999; *Satheesh and Ramanathan*, 2000; *Ramanathan et al.*, 2001].

[4] In this paper we examine the physical, chemical and radiative properties of aerosols over the Indian Ocean based on a variety of ground-based measurements made principally from Kaashidhoo Climate Observatory (KCO) as well as data available from the two other surface stations. Aerosol properties are modeled and their subsequent incorporation into a radiative transfer model faithfully reproduced the observed aerosol optical properties and radiative fluxes. The effect of sea-surface winds in modifying the aerosol forcing is examined and the results are discussed.

2. Experimental Setup and Data

[5] Extensive measurements are carried out at KCO, established in 1998 by Center for Clouds, Chemistry and Climate (C⁴), as a part of the INDOEX at Kaashidhoo island of Republic of Maldives (see *Ramanathan et al.* [1995, 1996, 2001] and *Satheesh et al.* [1999] for more details). Pre-INDOEX cruises during 1996 and 1997 and the first field phase (FFP) during 1998 have clearly established that sulfate and other continental aerosols are transported thousands of kilometers into the equatorial Indian Ocean (as far south as 5°S). These aerosol particles cause a significant reduction in solar radiation at the ocean surface [*Moorthy et al.*, 1997; *Satheesh et al.*, 1998; *Jayaraman et al.*, 1998; *Krishnamurti et al.*, 1998; *Meywerk and Ramanathan*, 1999]. The KCO is down wind of the Indian Subcontinent and is influenced by two contrasting air masses (continental and marine) associated with the Indian monsoon system. January to March was the experimental period during which the winds are mostly calm, and northeasterly (i.e., from the

landmass) associated with the winter monsoon (also called the northeast monsoon). This weather pattern becomes established toward the end of November and continues till April [*Das*, 1986; *Ramanathan et al.*, 1996, 2001].

[6] A list of instruments used at KCO, along with their specifications, are presented in Table 1. A detailed description of these instruments is given elsewhere [*Holben et al.*, 1998; *Satheesh et al.*, 1999; *Meywerk and Ramanathan*, 1999; *Conant*, 2000; *Ramanathan et al.*, 2001].

[7] AERONET Sun photometer is an auto tracking solar radiometer, which measures the field-limited solar radiation at eight narrow spectral bands from 340 to 1020 nm. The band at 940 nm is used for estimating the columnar water content and the other seven are used for the study of aerosols. The field-of-view (which determines the amount of diffuse radiation entering into the radiometer) of the radiometer is 1.2 degrees. This is small enough that the error caused by the diffuse light entering into the CIMEL's field of view should be less than 1% when the relative air mass (a geometrical term to account for the relative increase in the optical path length as solar zenith angle increases) is less than 2.0. The resulting uncertainty in the measured aerosol optical depth is less than ±0.01. More details about the AERONET radiometer are given by *Holben et al.* [1998] and *Eck et al.* [2001].

[8] In addition to KCO, optical depths were regularly estimated at two stations upwind of KCO for several years as part of Indian Space Research Organisation's Geosphere Biosphere Programme (ISRO-GBP) to characterize aerosols in that region. One of the stations, Minicoy (8.5°N, 73°E), is located about 400 km north of KCO. The other, Trivandrum (8.5°N, 77°E), is located on the mainland about 500 km due east of Minicoy. Identical instruments were in regular operation since 1993 at Trivandrum and since 1995 at Minicoy (see *Moorthy et al.* [1999] for details). The instrument used at these stations was a Multiwavelength solar Radiometer (MWR) designed and developed at the Space Physics Laboratory (SPL) following the principle of filter-wheel radiometers [*Shaw et al.*, 1973; *Moorthy et al.*, 1997, 1999]. The MWR measures the field limited direct solar flux at 10 narrow wavelength bands (from 380 to 1025 nm) as a function of solar zenith angle. The MWR system has a field of view of ~2.1°. The total columnar atmospheric optical depth at these wavelengths is estimated from the
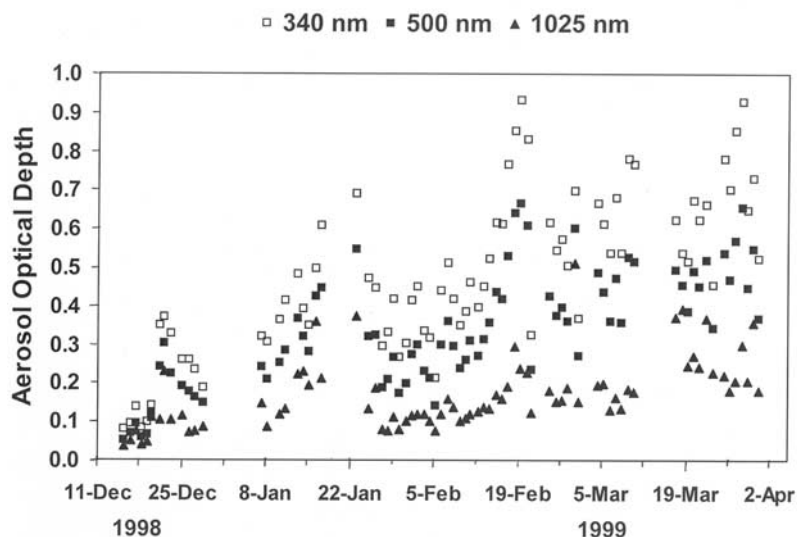
Figure 1. Variation of aerosol optical depth at three wavelengths: 340 (open squares), 500 (solid squares), and 1025 nm (open triangles).

MWR data following the Langley technique [*Shaw et al.*, 1973] and details are available elsewhere [*Moorthy et al.*, 1997; *Moorthy and Satheesh*, 2000].

3. Results and Discussion

3.1. Microphysical and Optical Properties

[9] The temporal variation of the aerosol optical depth at three representative wavelengths (UV, visible and near IR regions) is shown in Figure 1 from KCO data. The large build up of aerosol optical depth was observed with time from January to April in both years, particularly in 1999. The increase is more significant at visible wavelengths compared to near IR wavelengths. The steep spectral dependence during northeast monsoon season (during the experiment) is due to the impact of submicrometer aerosols (possibly from anthropogenic sources) from the continents from where winds arrive at KCO. Scattering of radiation by aerosols at a given wavelength is strongly dependent on the aerosol size. As a result, the temporal and spatial variations in the spectral dependence of optical depths are indicative of variations in the ambient aerosol size distribution. In the absence of large concentrations of airborne dust and sea salt particles, visible wavelengths are strongly influenced by submicrometer aerosols, which are often of anthropogenic origin. At KCO, the aerosol optical depth at 500 nm varies from ∼0.25 in January to ∼0.45 in March (Table 2). Aerosol optical depth does not change significantly from January to March at MCY (Table 2). Back trajectory analysis show that typically MCY was influenced by air masses from the Arabian peninsula and Sahara whereas KCO was influenced by air masses from the west coast and central region of India.

[10] The spectral values of aerosol optical depth contain information about aerosol size distribution. The simplest way to describe aerosols size information is by using Angstrom power law given by,

$$\tau_a = \beta\lambda^{-\alpha} \qquad (1)$$

where α is the wavelength exponent, β is the turbidity parameter and λ is the wavelength in μm. The value of α depends on the ratio of the concentration of large to small aerosols and β represents the total aerosol loading in the atmosphere [*Shaw et al.*, 1973]. The values of α and β are obtained by least squares fitting of the measured spectral optical depths in a log-log scale. An increase in α implies increase in the relative dominance of small aerosols and which in turn indicates anthropogenic influence (as most of the aerosols from anthropogenic sources are in the submicrometer range). A comparison of τ_a, α and β observed at KCO and Minicoy are shown in Table 2. At KCO, the value of α increases substantially from January to March, clearly demonstrating the anthropogenic impact from the Indian subcontinent. Such systematic variation is not observed in MCY and Trivandrum. The high values of α (>1.0 most of the time) at this island location far away from the continents is surprising since the spectral variation of aerosol optical depth over oceanic regions are typically less and at a lower value of α (<0.6) [*Satheesh and Moorthy*, 1997]. In our study the value of α was always larger than 0.6 and remained between 1.0 and 1.2.

[11] The concentration and vertical distribution of aerosol particles are important factors affecting the magnitude of the aerosol effect on radiation budget [*Kristament et al.*, 1993]. The role of aerosols in climate forcing also depends on the underlying surface of the Earth [*Heintzenberg et al.*, 1997]. The impact of aerosols on climate forcing is significantly

Table 2. Comparison of Aerosol Properties

Parameter	Station	Jan	Feb	Mar
τ_a	KCO	0.25	0.32	0.45
	MCY[a]	0.34	0.21	0.42
α	KCO	0.8	1.1	1.3
	MCY[a]	1.2	1.1	1.4
β	KCO	0.2	0.18	0.19
	MCY*	0.15	0.16	0.15

[a]Average of 1995 to 1998 (January to March).

different depending on whether the aerosol is concentrated above or below clouds. Thus knowledge of the vertical distribution of aerosols is critical. In addition, estimating column optical depths by vertically integrating the extinction coefficient requires knowledge of the vertical distribution of aerosol particles.

[12] The vertical distribution of aerosols are inferred using Lidar data (described by *Ansmann et al.* [2000]) as well as data from the National Center for Atmospheric Research (NCAR) C-130 aircraft (described by *Ramanathan et al.* [2001]). The aircraft was equipped with instruments to measure aerosol scattering and absorption coefficients. Examples of Lidar and aircraft measured extinction profiles are shown by *Ramanathan et al.* [2001]. Typically, two types of vertical distributions were observed: one in which the aerosol is concentrated in the boundary layer and another in which an elevated layer is observed near ~2 to 3 km [*Ansmann et al.*, 2000; *Ramanathan et al.*, 2001]. Because of uncertainties in the Lidar and aircraft data, we did not use the measured values directly. Rather, we normalized the values at each altitude using column aerosol optical depth obtained from vertically integrating the profile and then multiplying it by the independently measured column aerosol optical depth from AERONET photometer. In other words, the measured vertical profile shape is normalized to an independently measured column optical depth. About two thirds of the time the aerosol layer at 2 to 3 km was present and one third of time the aerosol layer was concentrated in the boundary layer [*Ramanathan et al.*, 2001].

[13] Size-segregated aerosol samples were collected at KCO and subsequently analyzed chemically at University of Miami, Florida, to obtain chemical composition. The flow of sample air was controlled by a wind sensor so that whenever air came from the island or the wind speed was less than 1 m s^{-1}, sampling was shut down to avoid contamination from local aerosol sources. The principal chemical species in the aerosol at KCO are sulfate, ammonium, nitrate, sea salt, soot, dust and organics. The insoluble portion of the aerosol is measured as ash after combustion of the sample filter [*Satheesh et al.*, 1999]. The measured ash is typically made up of mineral dust particles and fly ash from combustion processes. In the marine environment, nitrate is typically found associated with sea salt [*Savoie and Prospero*, 1982]. At KCO, nitrate had a substantial supermicrometer fraction. Thus we grouped sea salt and nitrate as single component [*Satheesh et al.*, 1999; *Ramanathan et al.*, 2001]. Chemical composition measurements showed that more than 80% of the sulfate and ammonium is in the submicrometer range, whereas less than 20% of the sea salt is in the submicron range. Since soot and organics were not measured at KCO, their values are obtained from coincident low altitude C-130 aircraft data from this region.

[14] The spectral extinction coefficient [$E_i(\lambda)$] of individual aerosol species are estimated using the Mie integral equation,

$$E_i(\lambda) = \int_{r_a}^{r_b} \pi r^2 Q_{ext}(m_i, r, \lambda) n_i(r) dr \qquad (2)$$

where Q_{ext} is the aerosol extinction efficiency factor which depends on the aerosol refractive index (m), aerosol radius

Aerosol Optical Depth (500 nm)
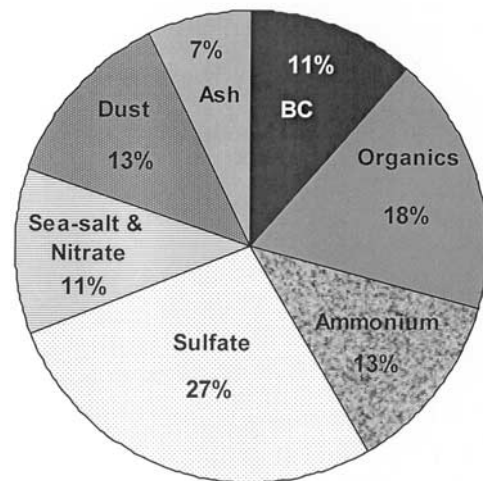
Figure 2. Percent contribution of different chemical species to the column aerosol visible optical depth.

(r) and the wavelength of incident radiation (λ); $n_i(r)$ is the measured aerosol size distribution; r_a and r_b are, respectively, the lower and upper radii limits of integration; and i represents different species. The corresponding column aerosol optical depths (τ_a) are obtained by vertically integrating the extinction coefficient (using the C-130 and Lidar profiles described before) [*Ramanathan et al.*, 2001].

[15] The dry aerosol properties are converted to ambient relative humidity following *Hess et al.* [1998]. The vertical variation of relative humidity obtained from radio sonde (RS) data is taken into account while estimating the aerosol optical depth. The aerosol optical depth estimated by adding the individual species optical depth are compared with the AERONET aerosol spectral optical depth for consistency in a similar fashion as described by *Satheesh et al.* [1999]. The percent contribution to τ_a of each chemical species is shown in Figure 2. Aerosol properties determined at sea level were integrated over the atmospheric column to estimate aerosol optical depth for each set of observations. One of the two types of aerosol vertical profiles (boundary layer or elevated layer type described in section 2) was used depending on the observation of the vertical distribution of aerosols. A complete flowchart is described in Figure 3.

3.2. Aerosol Radiative Effects: Observations Versus Model Results

[16] The aerosol properties described above are incorporated in a Monte Carlo radiative transfer model [*Podgorny et al.*, 1998, 2000] to estimate the broadband fluxes (for the wavelength bands corresponding to each instrument) at the surface and the top of the atmosphere (TOA). The band from 0.2 to 4.0 μm is divided into 38 narrow bands. The percentage contribution of different species to the aerosol optical depth (Figure 2) and SSA are estimated for these 38 band centers. The composite aerosol single scattering albedo (SSA) is given by

$$\omega_\lambda = \left(\frac{\omega_{1\lambda} E_{1\lambda} + \omega_{2\lambda} E_{2\lambda} + \omega_{3\lambda} E_{3\lambda} + \dots}{E_{1\lambda} + E_{2\lambda} + E_{3\lambda} + \dots} \right) \qquad (3)$$

```
┌─────────────────────────┐
│  Size Segregated Aerosol │
│   Chemical Composition   │
└─────────────────────────┘
            │
            ▼
┌─────────────────────────┐
│   Spectral Extinction    │
│  Coefficients of Various │
│     Aerosol Species      │
└─────────────────────────┘
            │
            ▼
┌─────────────────────────┐
│  Vertical Integration of │
│     the the Extinction   │
│  Coefficients using C-130│
│      and Lidar Profiles  │
└─────────────────────────┘
            │
            ▼
┌─────────────────────────┐
│  Comparison of Aerosol   │
│  Optical Depth with that │
│    Measured (AERONET)    │
└─────────────────────────┘
            │
            ▼
┌──────────────┐  ┌──────────────────────┐  ┌──────────────┐
│Spectral Single│ │Percent Contribution of│ │Column Water  │
│Scattering Albedo│ Various Species to    │ │   Vapour     │
│& Phase Function│ │Aerosol Optical Depth  │ │              │
└──────────────┘  └──────────────────────┘  └──────────────┘
            │              │                      │
            └──────────────┼──────────────────────┘
                           ▼
              ┌─────────────────────────┐
              │      Monte Carlo        │
              │   Radiative Transfer    │
              └─────────────────────────┘
                           │
                           ▼
              ┌─────────────────────────┐
              │      Surface & TOA       │
              │         Fluxes           │
              └─────────────────────────┘
```

Figure 3. Block diagram showing the procedure of estimating the aerosol optical properties and subsequent incorporation into radiative transfer model.

where $\omega_{1\lambda}$, $\omega_{2\lambda}$, $\omega_{3\lambda}$ etc are the single scattering albedos obtained from *Hess et al.* [1998] and $E_{1\lambda}$, $E_{2\lambda}$, $E_{3\lambda}$ etc are the extinction coefficient of individual aerosol species. The Monte Carlo radiative transfer model is used, because it allows us to treat each aerosol species explicitly. The absorption due to water vapor and CO_2 are estimated by using ESFT (exponential sum fitting of transmissions) coefficients and that due to O_2 and O_3 by using the corresponding spectral absorption coefficients [*Shi*, 1994]. The zenith-angle dependent ocean albedo is taken from *Breigleb et al.* [1986]. The spectral optical depths and column water vapor (from RS profiles) are used as input. Each of the chemical species is treated separately by using the corresponding spectral phase functions and single scattering albedos for individual species [*Hess et al.*, 1998]. Since sea salt and the component which consists of non-sea salt sulfate and ammonium are hygroscopic, different phase functions are used for different levels based on radio sonde profiles [*Satheesh et al.*, 1999].

[17] A comparison of the observed and model surface fluxes is shown in Figure 4. For both the cases (diffuse and global), modeled values are in good agreement with observed values. The comparison shown here used wavelength-dependent single scattering albedos and phase functions for the simulation of fluxes and is more accurate than a model using a single SSA and phase function to represent the whole wavelength band used earlier. The spectral fluxes at the surface are also simulated using a radiative transfer model and are compared with the observed spectral fluxes (using spectroradiometer at KCO; listed in Table 1) at the surface (Figure 5). The excellent agreement seen in Figures 4 and 5 gives a strong confirmation of the accuracy of the aerosol properties presented here.

[18] We compared the TOA clear-sky albedo from CERES (onboard TRMM) with model results from KCO. The CERES has a low inclination orbit and we get only one daytime measurement over the Arabian Sea (CERES on TRMM has a 10-km resolution at nadir where as the CERES instruments on Terra and Aqua have a 20-km resolution since the Terra and Aqua spacecraft orbits are approximately $2\times$ higher than TRMM). The following criteria were used to select the CERES data: (1) The time of CERES clear sky measurement should match the time of KCO clear sky data within 15 min, and (2) the spatial location of CERES clear sky pixel should be within 25 km of KCO. Figure 6 shows the CERES TOA albedo along with the model values as a function solar zenith angle. The data and model albedos are in excellent agreement (Figure 6), when the solar and satellite angles are less than $50°$. For the few data points when these angles exceed $50°$

INDOEX-Intensive Field Phase 1999
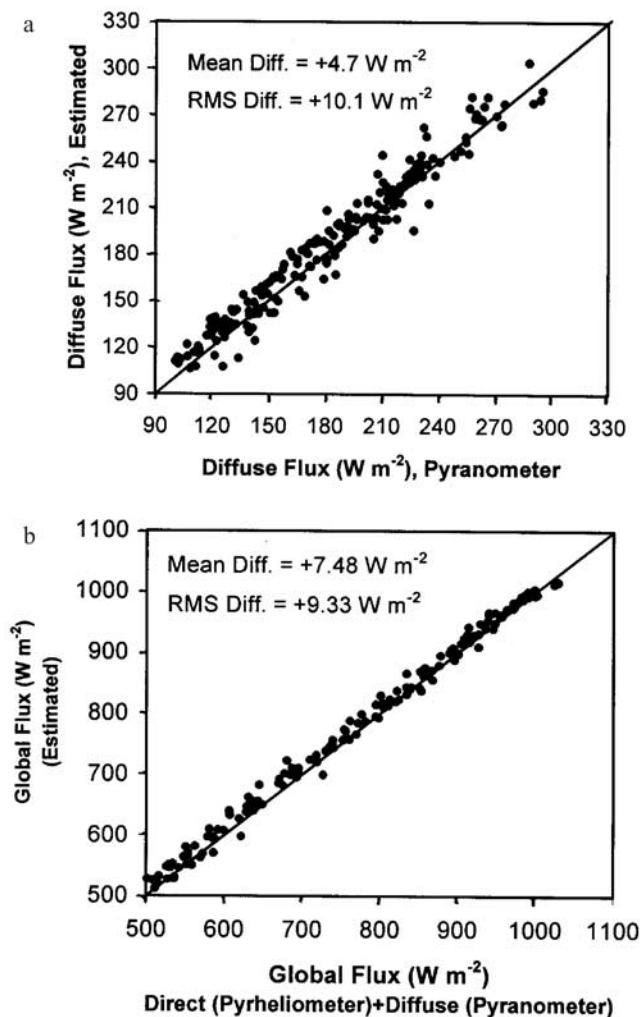
Figure 4. Comparison of measured and estimated surface (broadband) (a) diffuse and (b) global fluxes (see text for details).

(slant angles), the differences exceed 0.03. This large difference could be a result of algorithms for converting satellite radiances to fluxes being particularly prone to errors for slant solar and viewing angles. In addition, cloud contamination of scenes is more likely for slant satellite viewing angles (note that there is a systematic difference, with CERES albedos always larger for the slant angles).

[19] Aerosol single scattering albedo estimates were made using an integrating nephelometer and a Particle/Soot Absorption Photometer (PSAP) (Table 1). The nephelometer measured aerosol scattering continuously. Scattering data was used only when local winds were from over the ocean unaffected by the island and >1 m s^{-1}. Sample-airflow in the PSAP was controlled such that measurements were only made when the locals winds satisfied the conditions listed above. The nephelometer measured dry aerosol scattering and had to be corrected for relative humidity.

Scattering measurements were corrected for truncation by adjusting the correction described by *Anderson and Ogren* [1998] for the geometry of the nephelometer used in this study. PSAP data was corrected for scattering and calibration according to *Bond et al.* [1999]. The modeled daily mean single scattering albedo are estimated (following equation (3)) from the daily measurements of aerosol chemical composition at KCO. The modeled and observed aerosol single scattering albedos are shown in Figure 7. The vertical bar represents the standard deviation of the daily mean measured values. The vertical bar in the upper right corner represents the average uncertainty in the estimated values. Both curves agree within uncertainty limits. The slight deviations between the two could be due to the assumptions involved in the modeled values. Figure 8 shows the comparison of the spectral variation of single scattering albedo estimated from AERONET with that estimated from model.

[20] In summary, the modeled fluxes are in excellent agreement with the observed fluxes at the surface and those at the TOA. The same is the case with the measured and modeled aerosol physical and optical properties. This supports the validity of the modeled aerosol chemical, microphysical, and radiative properties reported here.

3.3. Excess Absorption?

[21] Recent studies suggest that the clear-sky atmosphere absorbs more short-wave radiation than predicted by radiative transfer models [*Arking*, 1996; *Kato et al.*, 1997; *Halthore et al.*, 1998]. These investigators observed that radiative transfer models consistently overestimate surface diffuse downward irradiance in a cloud-free atmosphere by 9 to 40% at low altitude sites while correctly calculating direct normal solar irradiance. Several investigators, on the other hand, found agreement in model-observed comparisons [*Cess et al.*, 1995; *Conant et al.*, 1998; *Kiehl et al.*, 1998]. The present study (section 3.2) shows agreement (Figure 4) between measured and modeled diffuse fluxes when measured aerosol properties are incorporated in to the radiative transfer model including absorbing components. Thus we do not find the need to invoke anomalous absorption to model diffuse fluxes.

3.4. Anthropogenic Contribution

[22] The contribution of various species to observed optical depth measurements is presented in Figure 2. Here we attempt to differentiate between natural and anthropogenic sources. In a remote marine location like Kaashidhoo, naturally occurring aerosols include sea salt from bubble bursting [*O'Dowd and Smith*, 1993; *Moorthy et al.*, 1997; *Moorthy and Satheesh*, 2000], airborne mineral dust, and non-sea salt sulfate produced by gas-to-particle conversion of precursor gases (e.g., dimethyl sulphide or DMS) emitted from the ocean. Sea Salt contributes 11% to τ_a (Figure 2); dust (assuming all of the measured ash is mineral dust) contributes another 12%.

[23] Non-sea salt sulfate can have both natural and anthropogenic sources. Measurements of methane sulfonic acid (MSA) from an earlier cruise in the Arabian Sea [*Krishnamurti et al.*, 1998] indicate that the DMS source is very small and accounts for <20% of the observed non-sea salt sulfate aerosol. Measurements of sulfate and am-
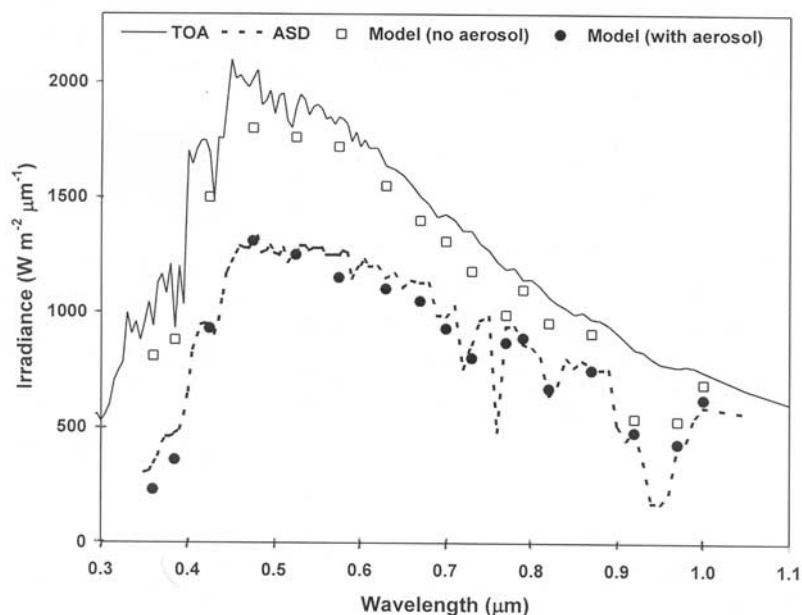
Figure 5. Comparison of modeled (solid circles) and measured (solid line) spectral flux at the surface. The open squares represent the modeled spectral flux with no aerosols.

monium at KCO show that the aerosol concentration of non-sea salt sulfate is about three times that of ammonium. Thus, out of the 38% for sulfate and ammonium, sulfate (DMS and anthropogenic) contribution is about 25%. If 20% of this sulfate is from natural sources (and the balance from industrial pollution from transport), we estimate that the natural source of sulfate contributes about 5% to τ_a. Since we used the upper limit for natural sources, the overall contribution of natural sources is likely less than 28% (11 + 12 + 5). Thus the anthropogenic portion of the total aerosol optical depth is >70%. It is possible, even likely that a fraction of the dust is anthropogenic (e.g., fly ash, road dust) making the anthropogenic contribution greater than estimated above.

3.5. Aerosol Forcing: External Versus Internal Mixing

[24] Aerosols modify incoming solar and outgoing IR radiation. Changes to radiation fluxes caused by aerosols is referred to as "radiative forcing." The effect of aerosols on TOA (top of the atmosphere) radiative fluxes is TOA radiative forcing and on surface radiative fluxes is the surface radiative forcing. The difference between the two is the atmospheric radiative forcing. In all cases, "aerosol forcing" is the difference in radiative fluxes with and without aerosols. Aerosol forcing can be estimated from both models and observations. The modeling approach incorporates measured aerosol properties into a radiative transfer model to estimate radiative fluxes with and without aerosols. The observational method compares measured radiative fluxes to those estimated using a model of an aerosol free atmosphere.

[25] In a recent study, following the above methods, *Satheesh and Ramanathan* [2000] reported the forcing efficiency (forcing per unit optical depth) at the surface to be in the range −70 to −75 W m^{-2} and that at the TOA to be −22 to −25 W m^{-2}. Table 3 summarizes aerosol forcing estimates at the surface for KCO based on a variety of

instruments and models. The range of the estimates is less than 10% of the mean, confirming the robustness of these surface-forcing estimates. The average aerosol optical depth observed at KCO was ∼0.4 during 1999, which when multiplied with the forcing efficiency yields the actual aerosol forcing over this region, i.e., ∼29 W m^{-2} at the surface and ∼10 W m^{-2} at the TOA.

[26] A number of studies address the effect of aerosol mixing state on radiative effects and report many different opinions [*Pilinis et al.*, 1995]. Most of the estimates of aerosol direct forcing due to absorbing aerosols assumed aerosols to be either externally mixed or well mixed components of an internal mixture. Numerous studies have shown this assumption not to be critical. *Pilinis et al.*
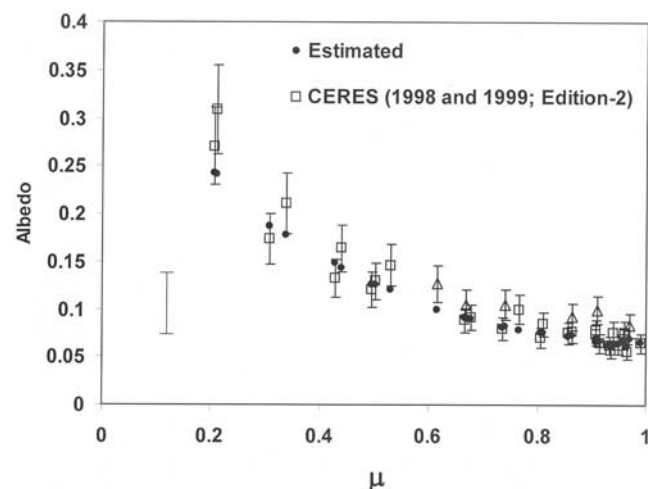
Figure 6. Comparison of the TOA albedo modeled (solid circles) and that measured by CERES satellite (open symbols). Open triangles represent that for satellite view angle greater than 60°.
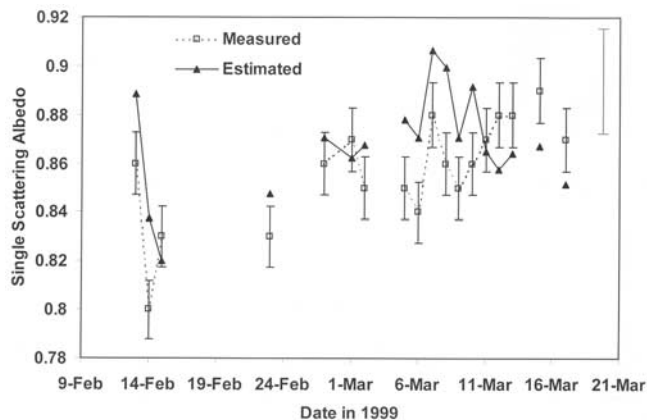
Figure 7. Comparison of surface single scattering albedo estimated (solid line) and measured using Nephelometer and PSAP (dashed line).

[1995], *McMurry et al.* [1996], and *Hignett et al.* [1999] all concluded that internal or external mixing is relatively unimportant when computing the total extinction due to aerosol. In reality, ambient aerosols likely exist in a state somewhere between completely externally mixed and completely internally mixed. Some investigators have hypothesized that reality is much closer to the internally mixed case [*Pilinis et al.*, 1995].

[27] In this section, we examine the effect of aerosol mixing state on the aerosol forcing using INDOEX data set. We first assume a completely externally mixed aerosol where each aerosol species is treated separately. Next, we assume a completely internally mixed aerosol where the complete aerosol system is treated as a single component. Volume weighted average refractive indices and single scattering albedos were used to estimate the optical and radiative properties for the internally mixed case. Surface forcing was about 2 W m^{-2} less for the internally mixed case compared to the externally mixed case. This difference is ∼6% of total surface forcing. TOA forcing is larger by ∼1.2 W m^{-2}, ∼12% of the total, for the internally mixed aerosol compared to the externally mixed case. The surface global fluxes from the two cases of mixing state agree within 0.5%. The maximum difference of ∼6 W m^{-2} was observed for overhead sun for both the global and the diffuse fluxes. Thus it appears that the mixing state of aerosols does not change aerosol forcing significantly. However, an aerosol in the form of a coated sphere made up of a solid inner core with an outer shell of different chemical composition may behave quite differently.

3.6. Role of Absorbing Aerosols

[28] The major absorbing aerosol components are soot and dust. Figure 2 indicates that soot contributes about 11% of the aerosol visible optical depth. Based on estimates of aerosol forcing by various aerosol species, soot appears to account for about 35% of surface forcing [*Podgorny et al.*, 2000]. During the beginning of the last decade, aerosols were generally thought to cool the planet and thus partly offset greenhouse warming [e.g., *Charlson et al.*, 1992; *Kiehl and Breigleb*, 1993; *Shaw et al.*, 1998; *Kiehl et al.*, 2000]. Recently, inclusion of realistic aerosol properties

(including aerosol absorption) in models indicate that aerosols cause less cooling than was commonly assumed [e.g., *Hansen et al.*, 1998]. Model calculations revealed that forcing can even be positive in the presence of absorbing aerosols [*Haywood and Shine*, 1995; *Haywood and Ramaswamy*, 1998; *Haywood et al.*, 1999]. Using an assumed soot/sulfate mass ratio, *Haywood and Shine* [1995] found carbonaceous soot within the troposphere can significantly modify clear-sky radiative forcing and reported a positive global mean forcing. They also found that positive forcing due to soot in the Northern Hemisphere reduces the interhemispheric difference in sulfate aerosol forcing. Several field experiments have found substantial amounts of carbonaceous aerosols [*Kaufman et al.*, 1998; *King et al.*, 1999; *Novakov et al.*, 1997, 2000].

[29] The ratio (f$_s$) of surface forcing to TOA forcing is an indicator of the amount of absorbing aerosols [*Satheesh and Ramanathan*, 2000]. Absorbing aerosols increase surface forcing and decrease TOA forcing; resulting in an increase in heating of the atmosphere. Higher ratios imply greater quantities of absorbing aerosols. The composite aerosol system includes both absorbing and nonabsorbing components. In our aerosol system, the absorbing components are soot and dust. The observed surface to TOA forcing ratio is ∼3. This ratio is much higher than that for pure sea-salt aerosols, ∼1.3, indicating the presence of absorbing aerosols. The value of f$_s$ becomes ∼1.9 when soot is removed from the system and, similarly, becomes ∼2.8 when dust is removed. The hypothetical cases of sea salt only and sulfate only aerosols yields an f$_s$ of ∼1.3 and 1.6 respectively. Thus the value of f$_s$ can vary from ∼1.3 to ∼3.5 depending on the amount of absorbing aerosols. On the other hand, when the sulfate is removed, the value of f$_s$ increased to ∼4.4, since no major component offsets the absorption of soot and dust. Model estimates of aerosol forcing at the surface and TOA have shown that sulfate contributes more to TOA forcing while soot contributes more to surface forcing [*Podgorny et al.*, 2000]. Elimination of the sulfate component in the model substantially decreases TOA forcing while having a relatively insignificant impact on surface forcing; thus increasing f$_s$.
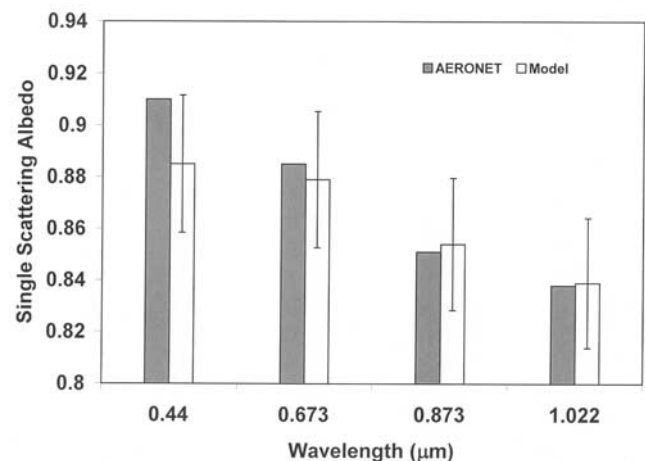
Figure 8. Comparison of spectral variation of single scattering albedo estimated from aerosol model (open bar) and estimated from AERONET measurements (shaded bar).

Table 3. Comparison of Various Forcing Estimates

Radiometer	Narrow Band/Broadband, f_e (S) (W m^{-2})	C_f^a	f_e (S),[b] W m^{-2}
Unshaded pyranometer[a]	−70	1.0	−70
Direct (pyrheliometer) + Diffuse (pyranometer)[c]	−73	1.0	−73
Photodiode Radiometer[d]	−40	1.73	−69.2
ASD Spectroradiometer	−55	1.35	−74.3
Model_0.90[e]	−70	1.0	−70
Model_0.87[e]	−76	1.0	−76

[a]C_f, Modeled ratio of broadband to narrow-band forcing efficiency.
[b]f_e(S), Broadband forcing efficiency.
[c]*Satheesh and Ramanathan*, 2000.
[d]*Conant*, 2000.
[e]Model_0.87 and Model_0.90 represent the modeled values using an SSA of 0.87 and 0.90, respectively.

[30] The bimodal nature of the aerosol size distribution indicates different aerosol sources contributing differently to the aerosol size. For example, the precursor gases emitted by anthropogenic activities form fine aerosols via gas-to-particle conversion processes, which contribute mainly to the submicron size. On the other hand, the aerosols produced by sea-spray or mineral dust contribute mostly to the supermicron size range. The effect of submicron and supermicron aerosols to the aerosol optical depth or radiative effects are different due to their size difference as well as their difference in chemical composition. The size distribution of accumulation and coarse mode aerosols are obtained by fitting unimodal lognormal distribution function to the submicron and supermicron modes separately. The accumulation mode thus obtained is mostly contributed by sulfates, ammonium, organics, soot and part of dust where as the coarse mode is contributed mainly by sea salt and part of dust. The single scattering albedo for the accumulation mode alone is estimated as ∼0.83 and coarse mode alone as ∼0.96. Table 4 shows the percent contribution in aerosol visible optical depth estimated for the accumulation and coarse mode separately at two representative wavelengths (0.5 and 1.0 μm). It can be seen that the major contributor at the visible region is accumulation mode aerosols and coarse mode shows little spectral variation and contributes significantly to the NIR wavelengths. The aerosol forcing (surface, atmosphere and TOA) estimated for the accumulation and coarse modes separately are also shown in Table 4.

3.7. Interannual Variability

[31] Aerosols are produced by a variety of processes and are variable in space and time. Aerosol properties at any given time and location depends on the relative strengths of various sources and sinks. In this section, we examine the temporal variation of aerosol properties using observations at three ground stations. Since KCO was established in February 1998, well after the other sites; observations from the other stations are used to characterize interannual variability. Figure 9 shows the interannual variability in aerosol optical depth over this region. In all years, aerosol optical depth peaks during March to May. This peak is also observed at KCO. However, the magnitude of this peak depends on the air mass trajectory of the air parcel arriving at KCO. For example, during IFP-1999, most air parcels traversed the Bay of Bengal before coming to KCO, instead of crossing the west-coast of India as they did during 1998. Simultaneous observations at KCO and MCY during February and March, 1998 show higher optical depths at MCY compared to KCO. This is quite reasonable since MCY is

much closer to the continent than KCO. Figure 9 also indicates that 1999 is not the only year during which the atmosphere over the Indian Ocean contained high levels of pollutants. For example, aerosol optical depths were high in 1996 and 1997 as well. The sun/sky radiometer observations made over the East Coast of United States in conjunction with TARFOX showed that the regional mean aerosol optical depth remained essentially constant for 1993 and 1996. Also, the lognormal aerosol size distribution parameters were almost identical for both years [*Remer et al.*, 1999]. Therefore, inter-annual variations may depend on local meteorological dynamics and may not affect all regions downwind of major source regions equally. Further, a doubling in optical depth from one year to another does not necessarily mean pollutant emissions also doubled. Rather, an increase in optical depth may only imply that pollutants are transported more efficiently to a particular location. Long-term observations (more than 15 years) over Trivandrum show that there is a gradual increase in aerosol visible optical depth from ∼0.2 in 1986 to ∼0.4 in 1999 (see Figure 10) [*Moorthy et al.*, 1999]. This means that aerosol optical depth increased on average ∼8% per year [*Parameswaran et al.*, 1998; *Moorthy et al.*, 1999]. This is not surprising as more than half of the world's population lives in Asia and economic developments in this region during the last decade resulted in huge increases in the number of industries and vehicles. For example, the number of vehicles increased from 2 million in 1970 to 38 million in 1998 (D. Chand, Physical Research Laboratory, Ahmedabad, private communication, 2001). Industrial emissions and anthropogenic activities such as biomass burning have created severe air pollution (aerosol haze) over most of the Asian region. Many of these processes produce substantial quantities of soot aerosols. A recent study has clearly shown the anthropogenic impact of soot over Indian region [*Suresh Babu and Moorthy*, 2001].

[32] The aerosol optical depth at KCO during 1999 was more than two times larger than during 1998 [*Satheesh and Ramanathan*, 2000]. The mean τ_a at 500 nm during 1999 was ∼0.4, while during 1998 the value was ∼0.16. The scattering and absorption coefficients also showed similar

Table 4. Percent Contribution

Mode/Property	Accumulation	Coarse
τ_p (0.5 μm)	65	35
τ_p (1.0 μm)	22	78
Surface forcing	75	25
Atmospheric forcing	83	17
TOA forcing	61	39
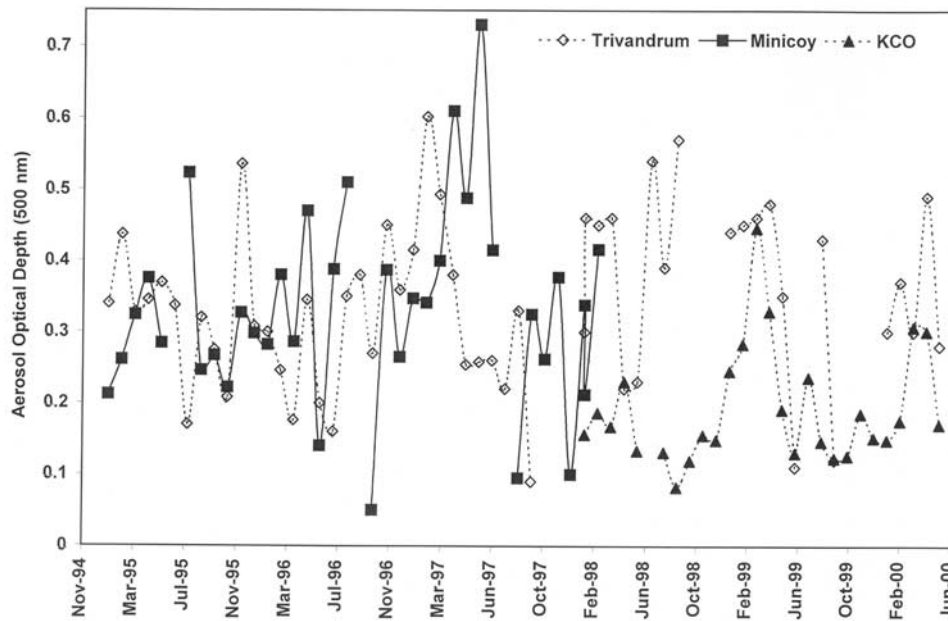
Figure 9. Interannual variation in aerosol optical depth. For the period prior to the KCO establishment (February 1998), the data from a nearby island, Minicoy island, are used.

increases. The aerosol single scattering albedo was in the range of 0.88 to 0.91 during 1998 while during 1999, it was in the range 0.86 to 0.88. Aerosol forcing changed as well. Surface forcing was in the range of -12 to -16 W m^{-2} during 1998 and -27 to -31 W m^{-2} during 1999. TOA forcing was in the range of -4 to -6 W m^{-2} during 1998 and -9 to -12 W m^{-2} during 1999. Aerosol forcing in each case was two times greater during 1999 than during 1998.

[33] In order to examine the seasonal variation of aerosol properties, the data is averaged into two sets: (1) average of November 98 to May 99 and (2) average of June 99 to October 99. The average values of aerosol optical depth and forcing are given in Table 5. It can be seen that the difference is significant in visible wavelengths compared to near IR wavelengths indicating the anthropogenic impact during November to May period. The aerosol absorption is $\sim$15 W m^{-2} during anthropogenically influenced period and $\sim$1 W m^{-2} during monsoon period (pristine air mass).

3.8. Role of Winds

[34] From Figure 2, it is clear that sea salt is a major contributor of natural aerosols (more than half of the natural). In this section we examine the role of sea-surface winds (which produce sea-salt aerosols) in modulating aerosol forcing.

[35] Observations of aerosol optical depth over tropical Indian Ocean show that aerosol optical depth increases with increasing sea-surface wind speed following an exponential relation of the form,

$$\tau_a = \tau_0 \exp(bU) \qquad (4)$$

where τ_a is the aerosol optical depth at wind speed U, b is a constant called "wind index" and τ_0 is aerosol optical depth at U = 0 [Moorthy et al., 1997]. The value of b depends on wavelength; b = 0.12 for λ = 0.5 μm and b = 0.18 for λ = 1.02

μm [Moorthy et al., 1997]. Since the production of aerosol species other than sea salt does not depend on wind speed, the enhancement of aerosol optical depth with increased surface wind speed is attributed to the local production of sea-salt aerosols. Comparison of aerosol optical depth and wind speed at KCO shows a similar correlation. However, the aerosol optical depth did not increase as rapidly with wind speed at KCO as in the previous study. The results are shown in Figures 11a and 11b.

[36] As wind speed increases two effects compete and determine aerosol forcing at the surface. Increased sea salt aerosols raise the single scattering albedo and increase the optical depth. Higher single scattering albedos decrease surface forcing efficiency, while greater optical depths increase forcing [Podgorny et al., 2000]. Alternately, at TOA, increases in both single scattering albedos and optical
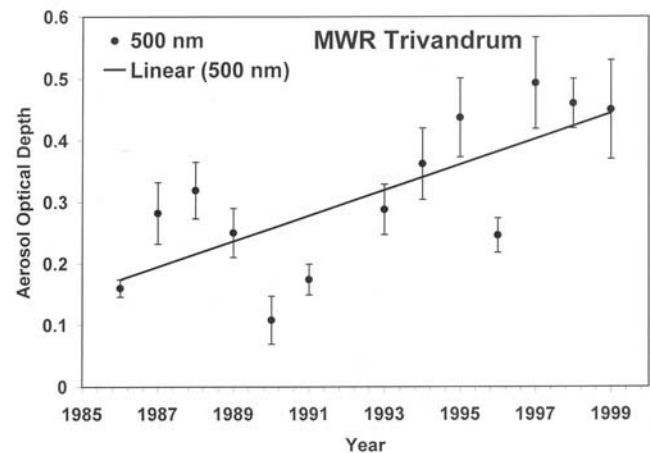
Figure 10. Long-term variations in aerosol optical depth from 1986 to 1999 measured at Trivandrum.

Table 5. Seasonal Variations

Period	τ_a (340 nm)	τ_a (500 nm)	τ_a (1020 nm)	F (S), W m^{-2}	F (T), W m^{-2}
November 1998 to May 1999	0.40 ± 0.09	0.28 ± 0.16	0.14 ± 0.09	21.0	6.7
June 1999 to October 1999	0.19 ± 0.07	0.14 ± 0.06	0.12 ± 0.06	6.3	5.5

depth increases aerosol forcing. A sea-surface wind speed increase from 0 to 15 m s^{-1} results in aerosol forcing at the TOA (negative) being enhanced by ~6 W m s^{-1} (i.e., larger negative value) [*Satheesh*, 2002]. In addition, surface winds have a significant role in determining the chemical composition of aerosols and hence the surface and TOA forcing. Model estimates of aerosol forcing in clear and cloudy skies have shown that aerosol forcing at the TOA decreases as cloud cover increases and can be positive when cloud coverage exceeds ~25%. A reflecting cloud layer causes both aerosol scattering and absorption effects to be amplified due to the multiple interactions of the radiation reflected back by clouds or between clouds and the surface. Thus the effect of the sea-surface winds is to offset (as the TOA forcing by sea-salt aerosol is negative or in other words net effect is cooling) part of the heating by soot aerosols.

[37] For many remote marine regions, sea-salt aerosols constitute most or nearly all of the total aerosol mass. In this case, any increase in sea-salt optical depth will be equal to the increase in total optical depth. Thus b (sea salt) is equal to b (total or composite aerosol). However, in a location where other aerosol types are important, such as KCO, where sea salt constitutes only 17% of total optical depth, any increase in sea salt will not change the total optical depth at the same rate. In this situation, b (total) < b (sea salt). This trend is consistent with the observed values of b at KCO-98, KCO-99 and MCY (Figure 11).

3.9. Aerosol Forcing Over Land

[38] The results reported so far were for observations over the ocean. The most significant differences between ocean and land as far as this study is concerned are the differences in specific heat capacities and surface reflectance. Land responds to surface radiation flux changes much more quickly than the ocean because of its lower heat capacity. However, during INDOEX, no calibrated surface flux measurements were made over land. Therefore, we present here a sensitivity study of the effect of aerosols over land in contrast to that over the ocean to assess the impact of aerosols over land. Aerosol concentrations tend to increase when approaching coastline from the open ocean [*Satheesh et al.*, 1998; *Jayaraman et al.*, 1998, 2001]. Since the sources of anthropogenic aerosols are located primarily on land, the concentrations of anthropogenic aerosols tend to be much larger over land than the open ocean. Unfortunately, no aerosol chemical composition measurements are available over the Indian continent during the study period. Consequently, we assume the same aerosol chemical composition for pollutant aerosols (from KCO observations) over land for this sensitivity study. One important disparity between land and ocean is the difference in surface albedo (reflectance). The average ocean albedo is ~6%, while over land it ranges from 15 to 35% or even more. Here we assume the extreme case of an albedo of ~35% to assess radiative forcing over land. The incorporation of the same aerosol composition into the radiative transfer model shows

that TOA forcing is positive over land. Aerosol forcing values over ocean and land are presented in Figure 12. The surface, atmospheric and TOA forcing implies an enhancement in lower atmosphere heating over land by about 40% simultaneous with a reduction of ~33% in surface cooling compared to that observed over ocean.

4. Summary and Conclusions

1. Extensive measurements of aerosol chemical and microphysical properties along with radiative fluxes were carried out in the haze plume off the Indian subcontinent.

2. The modeled and measured radiative fluxes at the surface and TOA showed good agreement when the measured aerosol properties (including absorbing components) are specified in the radiative transfer model. We did not need to invoke anomalous absorption to accurately model diffuse fluxes.
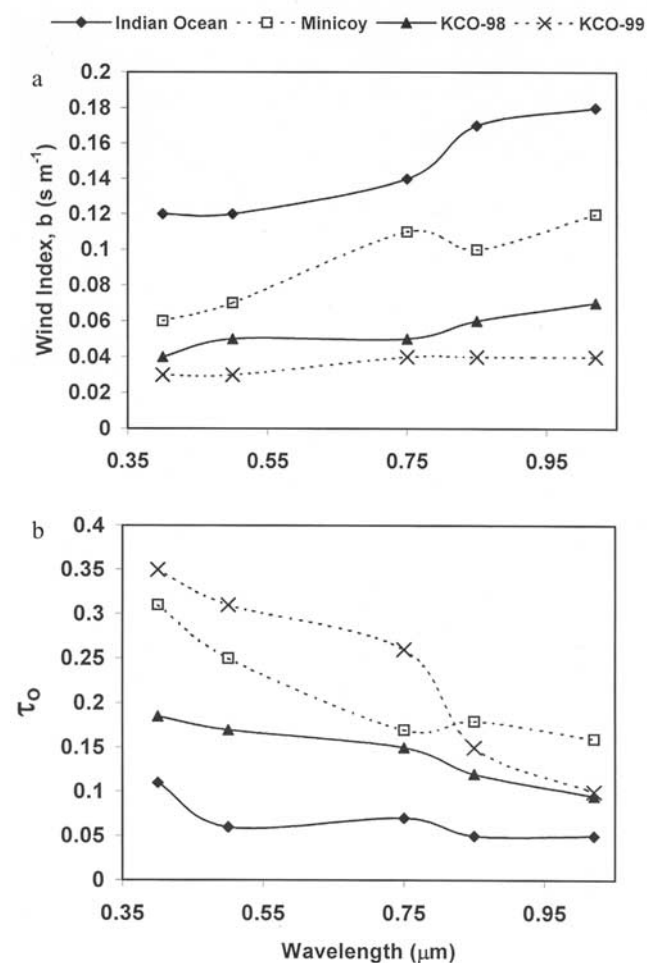
Figure 11. Spectral variation of wind index and wind independent aerosol optical depth.
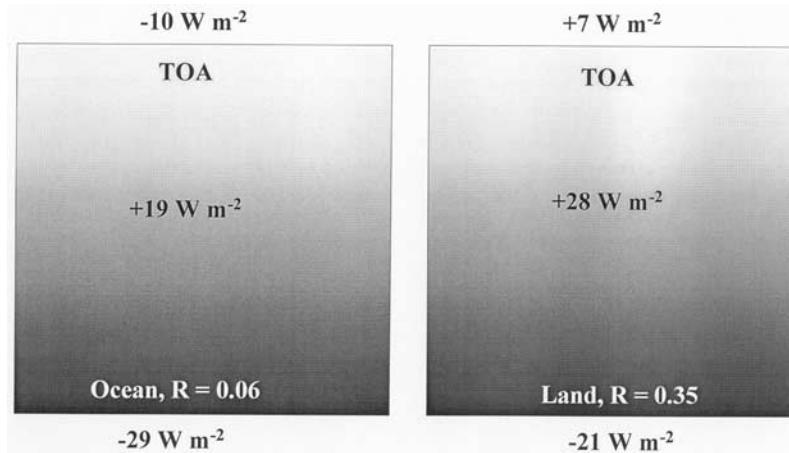
Figure 12. Effect of aerosols on short-wave radiation budget over land.

3. Aerosol mixing state (internal versus external mixtures) was found to be unimportant to radiative fluxes and aerosol forcing. However, if the aerosol exists as concentric spheres of disparate materials, the effect may be significant.

4. Anthropogenic sources contribute more than 70% to the aerosol visible optical depth.

5. Interannual variability in aerosol optical depth and forcing are significant.

6. Comparing observations at KCO, Minicoy and over the open ocean, indicates that increasing surface winds which produce higher concentrations of sea salt aerosols partly offsets the warming caused by absorbing aerosols.

7. A sensitivity study of the effect of aerosols over land versus over the ocean shows an enhancement in lower atmosphere heating by about 40% over land and a simultaneous reduction of ~33% in surface cooling.

References

Anderson, T. L., and J. A. Ogren, Determining aerosol radiative properties using the TSI 3563 integrating nephelometer, *Aerosol Sci. Technol.*, *29*, 57–69, 1998.

Ansmann, A., et al., Vertical profiling of the Indian aerosol plume with six-wavelength lidar during INDOEX: A first case study, *Geophys. Res. Lett.*, *27*, 963–966, 2000.

Arking, A., Absorption of solar energy in the atmosphere: Discrepancy between model and observations, *Science*, *273*, 779–782, 1996.

Bond, T. C., T. L. Anderson, and D. Campbell, Calibration and intercomparison of filter-based measurements of visible light absorption by aerosols, *Aerosol Sci. Technol.*, *30*, 582–600, 1999.

Breigleb, B. P., P. Minnis, V. Ramanathan, and E. Harrison, Comparison of regional clear-sky albedos inferred from satellite observations and model computations, *J. Clim. Appl. Meteorol.*, *25*, 214–226, 1986.

Cess, R. D., et al., Absorption of solar-radiation by clouds: Observations versus models, *Science*, *267*, 496–499, 1995.

Chameides, W. L., et al., A case study of the effects of atmospheric aerosols and regional haze on agriculture: An opportunity to enhance crop yields in China through emission controls?, *Proc. N.Y. Acad. Sci.*, *96*, 13,626–13,633, 1999.

Charlson, R. J., S. E. Schwartz, J. M. Hales, R. D. Cess, J. A. Coakley, J. E. Hansen, and D. J. Hoffmann, Climate forcing by anthropogenic aerosols, *Science*, *255*, 423–430, 1992.

Conant, W. C., An observational approach for determining aerosol surface radiative forcing: Results from the first field phase of INDOEX, *J. Geophys. Res.*, *105*, 15,347–15,360, 2000.

Conant, W. C., A. Vogelmann, and V. Ramanathan, The unexplained solar absorption and atmospheric H_2O: A direct test using clear-sky data, *Tellus, Ser. A*, *50*, 525–533, 1998.

Das, P. K., *The Monsoons*, 5th IMO lecture, *WMO 613*, World Meteorol. Organ., Geneva, 1986.

Eck, T. F., et al., Column-integrated aerosol optical properties over the Maldives during the northeast monsoon for 1998–2000, *J. Geophys. Res.*, *106*, 28,555–28,566, 2001.

Halthore, R. N., S. Nomesure, S. E. Schuartz, D. G. Imre, and A. Berk, Models overestimate clear-sky surface irradiance: A case for excess atmospheric absorption, *Geophys. Res. Lett.*, *25*, 3591–3594, 1998.

Hansen, J. E., M. Sato, A. Lacis, R. Ruedy, I. Tegen, and E. Matthews, Climate forcings in the Industrial era, *Proc. Natl. Acad. Sci.*, *95*, 12,753–12,758, 1998.

Haywood, J. M., and V. Ramaswamy, Global sensitivity studies of the direct radiative forcing due to anthropogenic sulfate and black carbon aerosols, *J. Geophys. Res.*, *103*, 6043–6058, 1998.

Haywood, J., and K. P. Shine, The effect of anthropogenic sulfate and soot aerosol on the clear sky planetary radiation budget, *Geophys. Res. Lett.*, *22*, 603–606, 1995.

Haywood, J. M., V. Ramaswamy, and B. J. Soden, Tropospheric aerosol climate forcing in clear-sky satellite observations over the oceans, *Science*, *283*, 1299–1303, 1999.

Heintzenberg, J., et al., Measurements and modeling of aerosol single scattering albedo: Progress, problems and prospects, *Beitr. Phys. Atmos.*, *70*, 249–263, 1997.

Hess, M., P. Koepke, and I. Schult, Optical properties of aerosols and clouds: The software package OPAC, *Bull. Am. Meteorol. Soc.*, *79*, 831–844, 1998.

Hignett, P., J. P. Taylor, P. N. Francis, and M. D. Glew, Comparison of observed and modeled direct aerosol forcing during TARFOX, *J. Geophys. Res.*, *104*, 2279–2287, 1999.

Holben, B. N., et al., AERONET-A federated instrument network and data archive for aerosol characterization, *Remote Sens. Environ.*, *66*, 1–16, 1998.

Intergovernmental Panel on Climate Change, *Climate Change 1994: Radiative Forcing of Climate, Report to IPCC*, Cambridge Univ. Press, New York, 1995.

Jayaraman, A., D. Lubin, S. Ramachandran, V. Ramanathan, E. Woodbridge, W. Collins, and K. S. Zalpuri, Direct observations of aerosol radiative forcing over the tropical Indian Ocean during the January–February 1996 pre-INDOEX cruise, *J. Geophys. Res.*, *103*, 13,827–13,836, 1998.

Jayaraman, A., S. K. Satheesh, A. P. Mitra, and V. Ramanathan, Latitude gradient in aerosol properties across the Inter-Tropical Convergence Zone: Results from the joint Indo-U.S. study onboard *Sagar Kanya*, *Curr. Sci.*, *80*, 128–137, 2001.

Kato, S., et al., Uncertainties in modeled and measured clear-sky surface shortwave irradiances, *J. Geophys. Res.*, *102*, 25,881–25,898, 1997.

Kaufman, Y. J., et al., Smoke, clouds, radiation–Brazil (SCAR_B) experiment, *J. Geophys. Res.*, *103*, 31,783–31,808, 1998.

Kiehl, J. T., and B. P. Breigleb, The radiative roles of sulfate aerosols and green house gases in climate forcing, *Science*, *260*, 311–314, 1993.

Kiehl, J. T., The National Center for Atmospheric Research Community Climate Model: CCM3, *J. Clim.*, *11*, 1131–1149, 1998.

Kiehl, J. T., T. L. Schneider, P. J. Rasch, M. C. Barth, and J. Wong, Radiative forcing due to sulfate aerosols from simulations with the National Center for Atmospheric Research Community Climate Model, Version 3, *J. Geophys. Res.*, *105*, 1441–1457, 2000.

King, M. D., Y. J. Kaufman, D. Tanre, and T. Nakajima, Remote sensing of tropospheric aerosols from space: Past, present, future, *Bull. Am. Meteorol. Soc.*, *80*, 2229–2259, 1999.

Krishnamurti, T. N., B. Jha, J. M. Prospero, A. Jayaraman, and V. Ramanathan, Aerosol and pollutant transport and their impact on radiative forcing over tropical Indian Ocean during the January–February, 1996 pre-INDOEX cruise, *Tellus, Ser. B*, *50*, 521–542, 1998.

Kristament, I. S., J. B. Liley, and M. J. Harvey, Aerosol variability in the vertical in the southwest Pacific, *J. Geophys. Res.*, *98*, 7129–7139, 1993.

Lelieveld, J., et al., The Indian Ocean Experiment: Widespread air pollution from South and Southeast Asia, *Science*, *291*, 1031–1036, 2001.

McMurry, P. H., X. Q. Zhang, and C. T. Lee, Issues in aerosol measurement for optics assessments, *J. Geophys. Res.*, *101*, 19,189–19,197, 1996.

Meywerk, J., and V. Ramanathan, Observations of the spectral clear-sky aerosol forcing over the tropical Indian Ocean, *J. Geophys. Res.*, *104*, 24,359–24,370, 1999.

Moorthy, K. K., and S. K. Satheesh, Characteristics of aerosols over a remote island, Minicoy in the Arabian Sea: Optical properties and retrieved size characteristics, *Q. J. R. Meteorol. Soc.*, *126*, 81–109, 2000.

Moorthy, K. K., S. K. Satheesh, and B. V. Krishma, Investigations of marine aerosols over tropical Indian Ocean, *J. Geophys. Res.*, *102*, 18,827–18,842, 1997.

Moorthy, K. K., et al., Aerosol Climatology over India, 1, ISRO GBP MWR network and data base, *ISRO GBP SR-03-99*, Indian Space Res. Organ., Bangalore, India, 1999.

Novakov, T., D. A. Hegg, and P. V. Hobbs, Airborne measurements of carbonaceous aerosols on the East Coast of the United States, *J. Geophys. Res.*, *102*, 30,023–30,030, 1997.

Novakov, T., T. S. Bates, and P. K. Quinn, Shipboard measurements of concentrations and properties of carbonaceous aerosols during ACE-2, *Tellus, Ser. B*, *52*, 228–238, 2000.

O'Dowd, C. D., and M. H. Smith, Physicochemical properties of aerosols over the northeast Atlantic: Evidence for wind speed related submicron sea-salt aerosol production, *J. Geophys. Res.*, *98*, 1137–1149, 1993.

Parameswaran, K., R. Rajan, G. Vijayakumar, K. Rajeev, K. K. Moorthy, P. R. Nair, and S. K. Satheesh, Seasonal and long term variations in aerosol content in the atmospheric mixing region at a tropical station in the Arabian Sea coast, *J. Atmos. Sol. Terr. Phys.*, *60*(1), 17–25, 1998.

Pilinis, C., S. N. Pandis, and J. H. Seinfeld, Sensitivity of direct climate forcing by atmospheric aerosols to aerosol size and composition, *J. Geophys. Res.*, *100*, 18,739–18,754, 1995.

Podgorny, I. A., A. M. Vogelmann, and V. Ramanathan, Effects of cloud shape and water vapor distribution on solar absorption in the near infrared, *Geophys. Res. Lett.*, *25*, 1899–1902, 1998.

Podgorny, I. A., W. C. Conant, V. Ramanathan, and S. K. Satheesh, Aerosol modulation of atmospheric and surface solar heating rates over the Tropical Indian Ocean, *Tellus, Ser. B*, *52*, 947–958, 2000.

Ramanathan, V., et al., Indian Ocean Experiment (INDOEX) white paper, report, Cent. for Clouds, Chem. and Clim., Scripps Inst. of Oceanogr., La Jolla, Calif., 1995. (Available at http://www-indoex.ucsd.edu)

Ramanathan, V., et al., Indian Ocean Experiment (INDOEX), A multi-agency proposal for field experiment in the Indian Ocean, *C4Publ. 162*, 83 pp., Cent. for Clouds, Chem. and Clim., Scripps Inst. of Oceanogr., La Jolla, Calif., 1996.

Ramanathan, V., et al., The Indian Ocean Experiment: An integrated analysis of the climate forcing and effects of the great Indo-Asian haze, *J. Geophys. Res.*, *106*, 28,371–28,398, 2001.

Remer, L. A., Y. J. Kaufman, and B. N. Holben, Interannual variation of ambient aerosol characteristics on the east coast of the United States, *J. Geophys. Res.*, *104*, 2223–2231, 1999.

Satheesh, S. K., Aerosol radiative forcing over tropical Indian Ocean: Modulation by sea-surface winds, *Curr. Sci.*, *82*, 310–315, 2002.

Satheesh, S. K., and K. K. Moorthy, Aerosol Characteristics over coastal regions of the Arabian Sea, *Tellus, Ser. B*, *49*, 417–428, 1997.

Satheesh, S. K., and V. Ramanathan, Large differences in the tropical aerosol forcing at the top of the atmosphere and Earth's surface, *Nature*, *405*, 60–63, 2000.

Satheesh, S. K., K. K. Moorthy, and B. V. K. Murthy, Spatial gradients in aerosol characteristics over the Arabian Sea and Indian Ocean, *J. Geophys. Res.*, *103*, 26,183–26,192, 1998.

Satheesh, S. K., V. Ramanathan, X. L. Jones, J. M. Lobert, I. A. Podgorny, J. M. Prospero, B. N. Holben, and N. G. Loeb, A model for the natural and anthropogenic aerosols for the tropical Indian ocean derived from Indian Ocean Experiment data, *J. Geophys. Res.*, *104*, 27,421–27,440, 1999.

Savoie, D. L., and J. M. Prospero, Particle size distribution of nitrate and sulfate in the marine atmosphere, *Geophys. Res. Lett.*, *9*, 1207–1210, 1982.

Shaw, G. E., J. A. Regan, and B. M. Herman, Investigations of atmospheric extinction using direct solar radiation measurements made with a multiple wavelength radiometer, *J. Appl. Meteorol.*, *12*, 374–380, 1973.

Shaw, G. E., R. L. Benner, W. Cantrell, and A. D. Clarke, The regulation of climate: A sulfate particle feedback loop involving deep convection –An editorial essay, *Clim. Change*, *39*, 23–33, 1998.

Shi, L., Cloud radiative forcing on surface short wave fluxes: A case study based on Cloud Lidar and Radar Exploratory Test, *J. Geophys. Res.*, *99*, 25,909–25,921, 1994.

Suresh Babu, S., and K. K. Moorthy, Anthropogenic impact on aerosol black carbon mass concentration at a tropical coastal station: A case study, *Curr. Sci.*, *81*, 1208–1214, 2001.

————————

B. N. Holben, Code 923, NASA Goddard Space Flight Center, Greenbelt, MD 20771, USA. (brent@aeronet.gsfc.nasa.gov)

N. G. Loeb, NASA Langley Research Center, Mail Stop 420, 21 Langley Boulevard, Hampton, VA 23681-0001, USA. (n.g.loeb@larc.nasa.gov)

H. Maring, J. M. Prospero, and D. Savoie, Rosenstiel School of Marine and Atmospheric Science, University of Miami, 4600 Rickenbacker Causeway, Miami, FL 33149, USA. (hmaring@rsmas.miami.edu; jprospero@ramas.miami.edu; dsavoie@rsmas.miami.edu)

K. K. Moorthy, Space Physics Laboratory, Vikram Sarabhai Space Centre, Trivandrum- 695 022, India. (k-k-moorthy@eth.net)

V. Ramanathan, Center for Clouds, Chemistry and Climate (C4), Scripps Institution of Oceanography, University of California, San Diego, 9500 Gilman Drive, La Jolla, CA 92093-0221, USA. (vram@fiji.ucsd.edu)

S. K. Satheesh, Centre for Atmospheric and Oceanic Sciences, Indian Institute of Science, Bangalore- 560 012, India. (satheesh@caos.lisc.ernet.in)